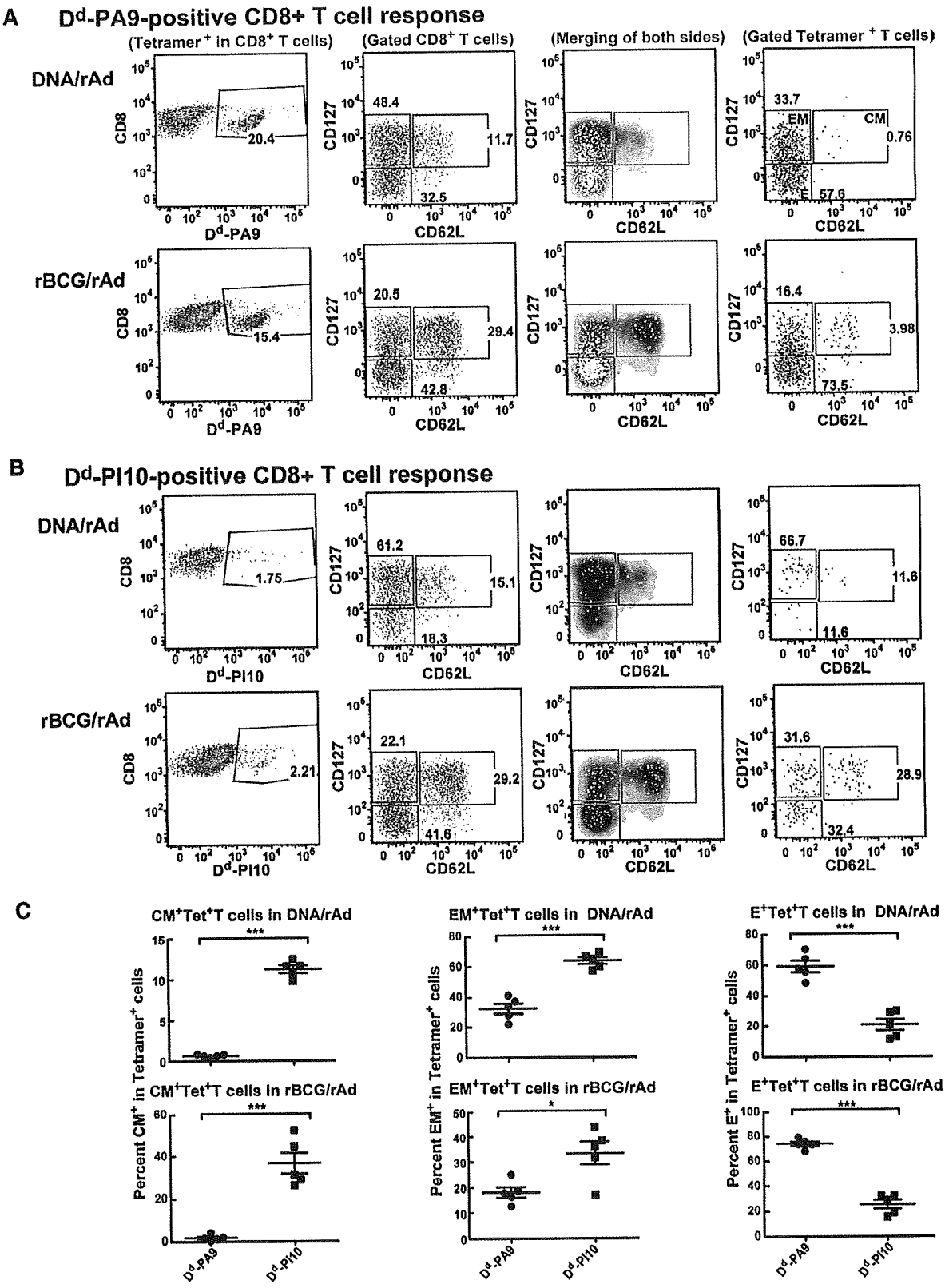

FIGURE 4. Phenotypes of D^d-PA9-specific and D^d-PI10-specific $CD8^+$ T cells elicited by immunization with DNA/rAd and rBCG/rAd. The differentiation phenotypes of tetramer-binding $CD8^+$ T cells specific for D^d-PA9 (*A*) and D^d-PI10 (*B*), harvested from the spleens of immunized mice at day 14 postboost (Fig. 3*C*), were analyzed by flow cytometry. Representative data are shown in *A* and *B*. The overall phenotypic distribution of the $CD8^+$ T cell population is shown in the *second column*; the *fourth column* shows the same analysis for the tetramer-positive events. Both sets of data are combined in the *third column*, which shows the tetramer-positive events (yellow) superimposed on the total $CD8^+$ T cell population (gray density cloud) in a bivariate plot of CD127 vs CD62L. *C*, Shows the phenotypic subset distribution of D^d-PA9-specific and D^d-PI10-specific $CD8^+$ T cells elicited by DNA/rAd (*upper panels*) and rBCG/rAd (*lower panels*) in each animal gated according to standard definitions. CM, $CD44^{high}CD127^{high}CD62L^{high}$; EM, $CD44^{high}CD127^{high}CD62L^{low}$; E (effector), $CD44^{high}CD127^{low}CD62L^{low}$. The CM cells were further defined to be $CCR7^+KLRG\text{-}1^{int}$ (data not shown).

D^d/PA9-#1

TCRBV	CDR3	TCRBJ	%	n
4	CASSTRQNAEQFF	2.1	100	81
TCRAV	**CDR3**	**TCRAJ**	**%**	**n**
16	CAMRGANYGNEKITF	48.01	84	21
16	CALRGANYGNEKITF	48.01	16	4

D^d/PA9-#2

TCRBV	CDR3	TCRBJ	%	n
4	CASSTRQNAEQFF	2.1	80	16
13	CASGDGGYTEVFF	1.1	15	3
13	CASSDLGRNYAEQFF	2.1	5	1
TCRAV	**CDR3**	**TCRAJ**	**%**	**n**
12	CALSDWPGANTGKLTF	52.01	47	9
14	CAENSGGSNYKLTF	53.01	16	3
13	CAIDPGTGSKLSF	58.01	16	3
14	CAAPPGFASALTF	35.02	10	2
6	CALVEGTGSKLSF	58.01	10	2

D^d/PI10-#1

TCRBV	CDR3	TCRBJ	%	n
1	CTCSADWGDTQYF	2.5	76	47
5	CASSQDNAGEVFF	1.1	13	8
13	CASGDAGVEQYF	2.7	6	4
29	CASSLSNAEQFF	2.1	5	3
TCRAV	**CDR3**	**TCRAJ**	**%**	**n**
4	CAADMDYANKMIF	47.01	46	21
13	CAMGNSGGSNYKLTF	53.01	24	11
16	CAMRESNNNAPRF	43.1	20	9
16	CAMREGGGNEKITF	48.01	4	2
16	CAMRESNNNAPKF	43.01	4	2
4	CVADMDYANKMIF	47.01	2	1

D^d/PI10-#2

TCRBV	CDR3	TCRBJ	%	n
13	CASIGQGAETLYF	2.3	28	9
13	CASKGLGDTGQLYF	2.2	13	4
13	CASAGGEGNTEVFF	1.1	9	3
4	CASSFGTGGNTLYF	1.3	6	2
13	CASGDGADQDTQYF	2.5	6	2
14	CASSSGTDQAPLF	1.5	6	2
13	CASSESGGPQDTQYF	2.5	6	2
13	CASRGQGMGQNTLYF	2.4	3	1
13	CASSDRPQDTQYF	2.5	3	1
29	CASSYAETLYF	2.3	3	1
29	CASSPPGQGYEQYF	2.7	3	1
13	CASMGGYAEQFF	2.1	3	1
14	CASSLHPRDWGGALEQYF	2.7	3	1
1	CTCSADWGDTQYF	2.5	3	1
17	CASSRGGNQDTQYF	2.5	3	1
TCRAV	**CDR3**	**TCRAJ**	**%**	**n**
9	CAVIEGGRALIF	15.01	17	2
13	CAMGNSGGSNYKLTF	53.01	8	1
12	CALSDQNTGYQNFYF	49.01	8	1
12	CALSCLPGTGSNRLTF	28.01	8	1
6	CALGALYGGSQNKLIF	32.02	8	1
12	CILRGTGGNNKLTF	56.01	8	1
6	CALGDHRIFF	31.01	8	1
7	CAASDLNNNNAPRF	43.02	8	1
14	CAARGYQNFYF	49.01	8	1
6	CVLGEPNTGKLTF	27.01	8	1
7	CASDSGYNKLTF	11.01	8	1

FIGURE 5. Clonotypic analysis of splenic $CD8^+$ T cells specific for D^d-PA9 and D^d-PI10. D^d/V3 peptide-specific tetramer-positive splenic $CD8^+$ T cells were sorted by flow cytometry 14 days after booster immunization with rAd in rBCG-primed animals; *TCR* gene expression was analyzed, as described in *Materials and Methods*. Clonotypes are shown in order of frequency for each sorted population with TCRBV/TCRAV usage, CDR3 sequences, and their TCRBJ/TCRAJ usage. Identical CDR3 amino acid sequences are color coded.

variation in the remaining residues. The complex with PA9 (Fig. 6, *A*, *D*, *G*, and *J*) shows exposure of peptide residues F7 and Y8, with the C-terminal A9 buried in the F pocket. With the additional residue found in the 10-mers, PI10 (Fig. 6, *B*, *E*, *H*, and *K*) and P18I10 (Fig. 6, *C*, *F*, and *I*), residues 6, 7, 8, and 9 buckle out. PI10 forms an aromatic stacking interaction between F7 and Y8, hiding much of Y8 from exposure to the TCR. P18I10, with the added flexibility of the additional residue, but lacking the potential for the aromatic stacking found in PI10, thrusts F7 back toward the α1 helix. Calculations of solvent-exposed surface area per peptide residue (Fig. S3) are consistent with the visual impression: PA9 exposes residues G4, A6, and Y8; PI10 exposes G4, A6, F7, and T9; and P18I10 exposes G4, A6, F7, and T9. These conformational differences may explain the difference in the binding of D^d-PI10,

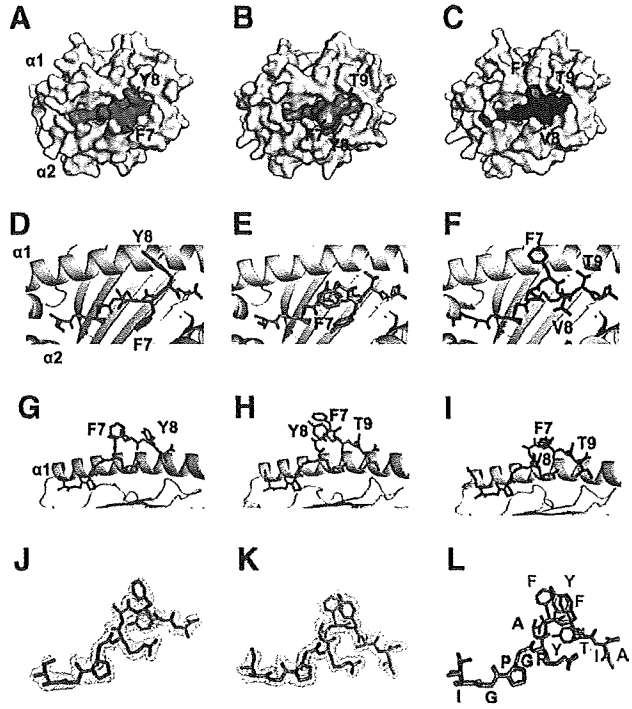

FIGURE 6. H-$2D^d$/peptide structures reveal distinct conformations of different bound peptides. Representations of x-ray structures of D^d-PA9 (*A*, *D*, and *G*), D^d-PI10 (*B*, *E*, and *H*), and D^d-P18I10 (*C*, *F*, and *I*) are shown in surface (*A–C*) and ribbon (*D–I*) representations. Peptides are colored cyan (PA9), orange (PI10), and magenta (P18I10). Viewpoint of *A–F* is from above, and of *G–L* from the side. Peptides PA9 and PI10, with accompanying electron density maps (contoured at 1σ), are shown in *J* and *K*. *L*, Shows the superposition of PA9 and PI10.

D^d-PA9, and D^d-P18I10 tetramers to specific $CD8^+$ T cells, and the differences in exposure of peptide residues 7, 8, and 9 between PA9 and PI10 offer a conceptual framework for possible differences in priming between PT9 and PT10 (see *Discussion*).

Discussion

Virus-specific $CD8^+$ T cells that arise after MHC-I-restricted presentation of peptides derived from the Env play a key role in the recognition of HIV-1-infected cells and in the control of virus replication. Although most viral proteins contain a large number of potential MHC-binding peptide epitopes, in general only a few of these epitopes evoke significant $CD8^+$ T cell responses. In a number of mouse strains, and also among human $CD8^+$ T cell responses, epitopes derived from the V3 loop of the HIV envelope are overrepresented (19, 33). In this study, we examined $CD8^+$ T cells elicited by different HIV-1_{BaL} vector vaccines using different H-$2D^d$/peptide tetramers. We suspected that the predicted immunodominant peptide of this isolate, PT10 (IGPGRAFYTT), or possibly the nonamer contained within, PT9 (IGPGRAFYT), might bind H-$2D^d$ with low affinity. Therefore, we explored the endogenous peptides as well as a set of related peptide variants for their ability to bind H-$2D^d$ in a MHC-I stabilization assay in TAP-deficient cells. Two additional peptides, PA9 and PI10, were selected for further comparative studies based on their ability to bind H-$2D^d$ (Fig. 1*B*) and elicit potent functional responses after immunization with HIV-1_{BaL} vector vaccines (Fig. S1).

What is the difference between these tetramer-specific $CD8^+$ T cell subsets? First, differences among these MHC-I/peptide complexes in the size of the exposed peptide loop as well as in the conformation of the exposed peptide present alternative targets for

TCR engagement. The difference in the reactivity of $CD8^+$ T cells specific for D^d-PI10 and D^d-PT10 is more subtle, but the finding that PT10 binds H-$2D^d$ with significantly lower affinity supports the view that it binds differently than PI10, and leads to the conclusion that the PT10 peptide is presented in a distinct conformation from PI10. Second, clear differences were apparent in the kinetics with which $CD8^+$ T cells specific for D^d-PI10 appeared relative to D^d-PA9-reactive $CD8^+$ T cells; these distinct mobilization kinetics confirm differential Ag recognition by D^d-PI10-specific and D^d-PA9-specific $CD8^+$ T cell populations. Several explanations are possible for these differential kinetics. One is that the proportion of D^d-PI10-reactive cells after priming is greater and that these expand more prominently following the boost. Another is that the D^d-PA9-reactive cells are of higher avidity for their cognate MHC/peptide complex, and, as shown in another model system (34–36), may eventually outcompete their lower avidity counterparts (37, 38). It is also possible that both mechanisms play a role in our immunization scheme, but additional experiments will be needed to assess both the relative proportion of reactive T cells as well as the relative avidity of these different $CD8^+$ T cell populations for their respective Ags.

The maturation and differentiation status (39, 40) of the two V3-specific tetramer-positive $CD8^+$ T cell populations was clearly different at the peak of the immune responses. D^d-PI10-specific $CD8^+$ splenocytes were CM rich, whereas the corresponding D^d-PA9-specific cells behaved much more like a primary population with higher peak effector cell numbers, thereby suggesting a greater degree of maturation and expansion. Together with the tetramer-specific double-staining profiles discussed above, it is apparent that HIV-1_{BaL} Env-specific immunodominant $CD8^+$ T cell responses are mediated by distinct V3 epitope-specific subsets, each with a different phenotype. It is noteworthy in this context that the ability of rAd vectors to generate CM seems to be important. In this mouse study, modeling the events that might be occurring in vaccinated humans, boosting DNA-primed animals with rAd induced more notable maturation of dominant D^d-PA9-specific $CD8^+$ T cells into effector cells. In contrast to this effector cell differentiation, generation of CM was significantly decreased in this immunization regimen. Lately, EM has been reported to be responsible for protection of animals from SIV challenge (36). Because low-dose rAd boosting increased the proportion of CM (data not shown) and because CM have been shown to expand in vivo and mediate protective immunity against pathogenic virus (39, 41), both low- and high-dose immunizations with rAd might be worth testing to determine whether one regimen will be preferable in generating more effective protective T cell immunity. In general, further studies in nonhuman primate challenge models will be needed to permit evaluation of the character of the T cell response that contributes to protection, and such studies have been initiated.

Of particular interest is the observation that the different Env vaccine/immunization regimens elicited $CD8^+$ T cell populations with different fine specificities and clonotype usage. The x-ray crystallographic analysis of the D^d-PA9 and D^d-PI10 complexes revealed a structural basis for these differences in peptide specificity, suggesting that alternative vaccination regimens lead to differences in Ag processing and presentation that in turn elicit distinct populations of Ag-specific T cells. Structural differences in the size of the exposed peptide loop (nonamer vs decamer) and in the conformation of the exposed peptide were apparent. Although we have been unable to obtain crystals of either D^d-PT9 or D^d-PT10, we speculate that D^d-PT9 has a stable peptide conformation very similar to that of D^d-PA9. D^d-PT10, however, lacking the strong p10 isoleucine anchor residue, may have at least two distinct conformations of the bound peptide, one with the position 9T down in the F pocket and the position 10T up exposed to solvent extending beyond the peptide-binding groove, and a second with the position 10T down in the F pocket. Such conformational dimorphism of MHC-I-bound peptides has been suggested by two different high resolution structures of HLA-B*2705, complexed with either pVIPR (RRKWRRWHL) (42) or pGR (RRRWHR WRL) (43). These two peptides have been reported to induce cross-reactive $CD8^+$ T cells.

The observation that distinct populations of T cells that recognize D^d-PA9, D^d-PT9, D^d-PT10, and D^d-PI10 are differently elicited by a single protein immunogen is reminiscent of the two different classes (types A and B) of hen egg lysozyme-specific $CD4^+$ T cells observed by Unanue and colleagues (44). Type A conventional T cells recognize a distinct conformation of the peptide/I-A^k complex generated in the presence of H2-DM in late endocytic vesicles, whereas type B cells identify a distinct conformation of the same peptide/I-A^k complex produced by peptide exchange in the absence of H2-DM. There clearly are differences in the MHC-II processing and presentation systems observed for hen egg lysozyme as compared with the Env vaccine systems that we have studied. However, the distinct T cell populations that we observe may be indicative of different conformations of peptide/MHC-I complexes generated by processing and presentation from different types of APC, by a cellular mechanism similar to that observed for hen egg lysozyme/I-A^k. Complex mechanisms of Ag processing and presentation, as well as variations in the T cell repertoire, play important roles in the variability and specificity of the Ag-specific T cell response (45, 46). The differences in Ag-specific $CD8^+$ T cell induction between the two prime-boost regimens are most likely due to differences in the priming Ags. The i.m. injection of plasmid DNA-encoding Env results in cellular gene expression, which typically leads to Ag processing through a proteasomal pathway (47). In contrast, the injected rBCG must enter an endosomal/lysosomal pathway to generate peptides for presentation by MHC-I (48). Thus, endogenously generated PT9 and PT10 may be presented differently in the context of H-$2D^d$ in different APC, and moreover, PT10 may be displayed in two distinct conformations (Fig. 7). Furthermore, this mechanistic explanation enables an understanding of the relative immunodominance profiles between D^d-PI10-specific and D^d-PA9-specific $CD8^+$ T cell populations. Differences in epitope abundance and compartmentalization (49), both temporally and between the different vaccination regimens, could explain the observed differential induction of $CD8^+$ T cells specific for D^d-PI10 and D^d-PA9.

Immunization to elicit protective T cell responses offers a reasonable strategy for design of vaccines against a variety of infectious diseases (50, 51), and MHC-I/peptide tetramers can be effective for evaluating not only the extent, but also the specificity of T cell immunity. The general approach to evaluating $CD8^+$ T cell-inducing vaccines in this study relied on several experimental strategies. First, we focused on the region of the immunizing envelope Ag known to elicit the immunodominant response. Second, we empirically tested a set of clade-specific and synthetic variant peptides for their ability to bind the known MHC-I-presenting molecule. Using both the optimal binding peptides and those that were putatively endogenously generated to produce H-$2D^d$ tetramers, we detected different $CD8^+$ T cell subsets specific for PI10 and PA9. Structural understanding of the MHC-I/peptide complex may facilitate our ability to identify Ag-specific $CD8^+$ T cell activation in vivo in response to vector-based vaccines. Such an approach toward exploring variant peptides for MHC-I binding and for tetramer production may allow broader detection of T cell responses to HIV-1.

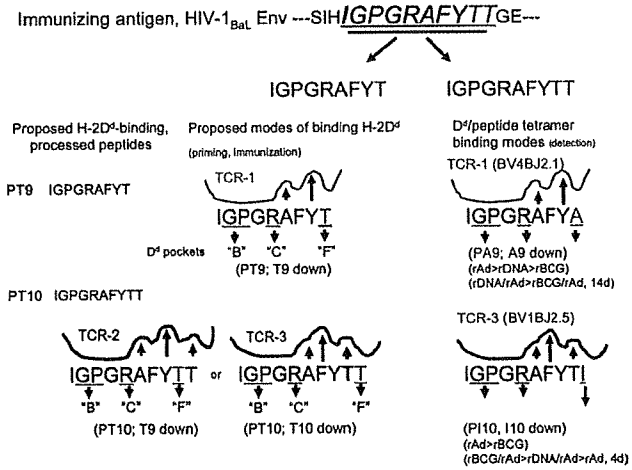

FIGURE 7. Model for differential priming of T cells with distinct fine specificity as revealed by tetramer binding. The model depicts the V3 loop peptide in HIV-1_{BaL} envelope glycoprotein, SIH*IGPGRAFYTT*GE, with the core H-2D^d-binding nonamer and decamer peptides (italics, underlined). PT9 and PT10, and their amino acid sequences, are shown. The orientation of the side chains of the H-2D^d-bound peptides is shown, as follows: 1) for PT9, one conformation is proposed; 2) for PT10, two alternative conformations are proposed, one with 9T down in the "F" pocket and one with 10T down. The TCRs are TCR-1, TCR-2, and TCR-3. Upward arrows indicate side chains most likely available for TCR interaction. The GP (gly-pro) "B" pocket anchor motif is underlined, with "F" pocket residues shown (downward arrows). Three different TCRs are indicated in different colors to emphasize their tetramer specificity. For each TCR (*right column*), the hierarchy of responses in single modality (*top*) or prime-boost (*second*) is indicated, as well as the day of peak response for the prime-boost regimen.

In summary, we have shown that different prime-boost vaccination regimens can elicit CD8$^+$ T cell responses with distinct specificity, cross-reactivity, clonotypic structure, and maturation. The immunodominant HIV Env-V3 responses were mediated by two distinct tetramer-specific CD8$^+$ T cell subpopulations. Together, these findings suggest the importance of an understanding of MHC-peptide binding and structure for the rational design of effective vaccines.

Acknowledgments

We thank Zhi-yong Yang, Dr. Barney Graham, and Dr. Robert Seder for valuable discussions, and Dr. N. Yamamoto for advice, support, and encouragement. We also thank Ian Meltzer and Kathryn Bonaparte for analysis of *TCRA* and *TCRB* gene expression, Stephen Perfetto and Richard Nguyen for assistance with flow cytometry, Srini Rao and Alida Ault for animal care, Jeff Skinner for biostatistical consultation, and Lisa Boyd as well as the National Institute of Allergy and Infectious Diseases MHC Tetramer Core Facility for preparation of MHC-I/peptide tetramers.

Disclosures

The authors have no financial conflict of interest.

References

1. Li, Y., S. A. Migueles, B. Welcher, K. Svehla, A. Phogat, M. K. Louder, X. Wu, G. M. Shaw, M. Connors, R. T. Wyatt, and J. R. Mascola. 2007. Broad HIV-1 neutralization mediated by CD4-binding site antibodies. *Nat. Med.* 13: 1032–1034.
2. Huang, C. C., S. N. Lam, P. Acharya, M. Tang, S. H. Xiang, S. S. Hussan, R. L. Stanfield, J. Robinson, J. Sodroski, I. A. Wilson, et al. 2007. Structures of the CCR5 N terminus and of a tyrosine-sulfated antibody with HIV-1 gp120 and CD4. *Science* 317: 1930–1934.
3. Fischer, W., S. Perkins, J. Theiler, T. Bhattacharya, K. Yusim, R. Funkhouser, C. Kuiken, B. Haynes, N. L. Letvin, B. D. Walker, et al. 2007. Polyvalent vaccines for optimal coverage of potential T-cell epitopes in global HIV-1 variants. *Nat. Med.* 13: 100–106.
4. Barouch, D. H., S. Santra, J. E. Schmitz, M. J. Kuroda, T. M. Fu, W. Wagner, M. Bilska, A. Craiu, X. X. Zheng, G. R. Krivulka, et al. 2000. Control of viremia and prevention of clinical AIDS in rhesus monkeys by cytokine-augmented DNA vaccination. *Science* 290: 486–492.
5. Shiver, J. W., T. M. Fu, L. Chen, D. R. Casimiro, M. E. Davies, R. K. Evans, Z. Q. Zhang, A. J. Simon, W. L. Trigona, S. A. Dubey, et al. 2002. Replication-incompetent adenoviral vaccine vector elicits effective anti-immunodeficiency-virus immunity. *Nature* 415: 331–335.
6. Graham, B. S., R. A. Koup, M. Roederer, R. T. Bailer, M. E. Enama, Z. Moodie, J. E. Martin, M. M. McCluskey, B. K. Chakrabarti, L. Lamoreaux, et al. 2006. Phase 1 safety and immunogenicity evaluation of a multiclade HIV-1 DNA candidate vaccine. *J. Infect. Dis.* 194: 1650–1660.
7. Harari, A., P. A. Bart, W. Stohr, G. Tapia, M. Garcia, E. Medjitna-Rais, S. Burnet, C. Cellerai, O. Erlwein, T. Barber, et al. 2008. An HIV-1 clade C DNA prime, NYVAC boost vaccine regimen induces reliable, polyfunctional, and long-lasting T cell responses. *J. Exp. Med.* 205: 63–77.
8. Mattapallil, J. J., D. C. Douek, A. Buckler-White, D. Montefiori, N. L. Letvin, G. J. Nabel, and M. Roederer. 2006. Vaccination preserves CD4 memory T cells during acute simian immunodeficiency virus challenge. *J. Exp. Med.* 203: 1533–1541.
9. Nabel, G. J. 2001. Challenges and opportunities for development of an AIDS vaccine. *Nature* 410: 1002–1007.
10. Letvin, N. L. 2007. Correlates of immune protection and the development of a human immunodeficiency virus vaccine. *Immunity* 27: 366–369.
11. Letvin, N. L., J. R. Mascola, Y. Sun, D. A. Gorgone, A. P. Buzby, L. Xu, Z. Y. Yang, B. Chakrabarti, S. S. Rao, J. E. Schmitz, et al. 2006. Preserved CD4$^+$ central memory T cells and survival in vaccinated SIV-challenged monkeys. *Science* 312: 1530–1533.
12. Reynolds, M. R., A. M. Weiler, K. L. Weisgrau, S. M. Piaskowski, J. R. Furlott, J. T. Weinfurter, M. Kaizu, T. Soma, E. J. Leon, C. MacNair, et al. 2008. Macaques vaccinated with live-attenuated SIV control replication of heterologous virus. *J. Exp. Med.* 205: 2537–2550.
13. Chen, W., S. Khilko, J. Fecondo, D. H. Margulies, and J. McCluskey. 1994. Determinant selection of major histocompatibility complex class I-restricted antigenic peptides is explained by class I-peptide affinity and is strongly influenced by nondominant anchor residues. *J. Exp. Med.* 180: 1471–1483.
14. Laugel, B., D. A. Price, and A. K. Sewell. 2006. On the path to TCR-directed therapeutics. *Nat. Biotechnol.* 24: 615–616.
15. Varela-Rohena, A., P. E. Molloy, S. M. Dunn, Y. Li, M. M. Suhoski, R. G. Carroll, A. Milicic, T. Mahon, D. H. Sutton, B. Laugel, et al. 2008. Control of HIV-1 immune escape by CD8 T cells expressing enhanced T-cell receptor. *Nat. Med.* 14: 1390–1395.
16. Letvin, N. L., Y. Huang, B. K. Chakrabarti, L. Xu, M. S. Seaman, K. Beaudry, B. Korioth-Schmitz, F. Yu, D. Rohne, K. L. Martin, et al. 2004. Heterologous envelope immunogens contribute to AIDS vaccine protection in rhesus monkeys. *J. Virol.* 78: 7490–7497.
17. Huang, C. C., M. Tang, M. Y. Zhang, S. Majeed, E. Montabana, R. L. Stanfield, D. S. Dimitrov, B. Korber, J. Sodroski, I. A. Wilson, et al. 2005. Structure of a V3-containing HIV-1 gp120 core. *Science* 310: 1025–1028.
18. Palker, T. J., M. E. Clark, A. J. Langlois, T. J. Matthews, K. J. Weinhold, R. R. Randall, D. P. Bolognesi, and B. F. Haynes. 1988. Type-specific neutralization of the human immunodeficiency virus with antibodies to *env*-encoded synthetic peptides. *Proc. Natl. Acad. Sci. USA* 85: 1932–1936.
19. Takahashi, H., R. Houghten, S. D. Putney, D. H. Margulies, B. Moss, R. N. Germain, and J. A. Berzofsky. 1989. Structural requirements for class I MHC molecule-mediated antigen presentation and cytotoxic T cell recognition of an immunodominant determinant of the human immunodeficiency virus envelope protein. *J. Exp. Med.* 170: 2023–2035.
20. Takahashi, H., S. Merli, S. D. Putney, R. Houghten, B. Moss, R. N. Germain, and J. A. Berzofsky. 1989. A single amino acid interchange yields reciprocal CTL specificities for HIV-1 gp160. *Science* 246: 118–121.
21. Bikoff, E. K., G. R. Otten, and E. J. Robertson. 1991. Defective assembly of class I major histocompatibility complex molecules in an embryonic cell line. *Eur. J. Immunol.* 21: 1997–2004.
22. Darrah, P. A., D. T. Patel, P. M. De Luca, R. W. Lindsay, D. F. Davey, B. J. Flynn, S. T. Hoff, P. Andersen, S. G. Reed, S. L. Morris, et al. 2007. Multifunctional TH1 cells define a correlate of vaccine-mediated protection against *Leishmania major*. *Nat. Med.* 13: 843–850.
23. Kozlowski, S., T. Takeshita, W. H. Boehncke, H. Takahashi, L. F. Boyd, R. N. Germain, J. A. Berzofsky, and D. H. Margulies. 1991. Excess β_2 microglobulin promoting functional peptide association with purified soluble class I MHC molecules. *Nature* 349: 74–77.
24. Betts, M. R., and R. A. Koup. 2004. Detection of T-cell degranulation: CD107a and b. *Methods Cell Biol.* 75: 497–512.
25. Precopio, M. L., M. R. Betts, J. Parrino, D. A. Price, E. Gostick, D. R. Ambrozak, T. E. Asher, D. C. Douek, A. Harari, G. Pantaleo, et al. 2007. Immunization with vaccinia virus induces polyfunctional and phenotypically distinctive CD8$^+$ T cell responses. *J. Exp. Med.* 204: 1405–1416.
26. Douek, D. C., M. R. Betts, J. M. Brenchley, B. J. Hill, D. R. Ambrozak, K. L. Ngai, N. J. Karandikar, J. P. Casazza, and R. A. Koup. 2002. A novel approach to the analysis of specificity, clonality, and frequency of HIV-specific T cell responses reveals a potential mechanism for control of viral escape. *J. Immunol.* 168: 3099–3104.
27. Li, H., K. Natarajan, E. L. Malchiodi, D. H. Margulies, and R. A. Mariuzza. 1998. Three-dimensional structure of H-2Dd complexed with an immunodominant peptide from human immunodeficiency virus envelope glycoprotein 120. *J. Mol. Biol.* 283: 179–191.

28. Emsley, P., and K. Cowtan. 2004. Coot: model-building tools for molecular graphics. *Acta Crystallogr. D. Biol. Crystallogr.* 60: 2126–2132.
29. Wu, L., W. P. Kong, and G. J. Nabel. 2005. Enhanced breadth of CD4 T-cell immunity by DNA prime and adenovirus boost immunization to human immunodeficiency virus Env and Gag immunogens. *J. Virol.* 79: 8024–8031.
30. Bergmann, C., S. A. Stohlmann, and M. McMillan. 1993. An endogenously synthesized decamer peptide efficiently primes cytotoxic T cells specific for the HIV-1 envelope glycoprotein. *Eur. J. Immunol.* 23: 2777–2781.
31. Corr, M., L. F. Boyd, E. A. Padlan, and D. H. Margulies. 1993. H-2Dd exploits a four residue peptide binding motif. *J. Exp. Med.* 178: 1877–1892.
32. Tormo, J., K. Natarajan, D. H. Margulies, and R. A. Mariuzza. 1999. Crystal structure of a lectin-like natural killer cell receptor bound to its MHC class I ligand. *Nature* 402: 623–631.
33. Wu, L., Z. Y. Yang, L. Xu, B. Welcher, S. Winfrey, Y. Shao, J. R. Mascola, and G. J. Nabel. 2006. Cross-clade recognition and neutralization by the V3 region from clade C human immunodeficiency virus-1 envelope. *Vaccine* 24: 4995–5002.
34. Welsh, R. M. 2006. Private specificities of heterologous immunity. *Curr. Opin. Immunol.* 18: 331–337.
35. Kedl, R. M., J. W. Kappler, and P. Marrack. 2003. Epitope dominance, competition and T cell affinity maturation. *Curr. Opin. Immunol.* 15: 120–127.
36. Hansen, S. G., C. Vieville, N. Whizin, L. Coyne-Johnson, D. C. Siess, D. D. Drummond, A. W. Legasse, M. K. Axthelm, K. Oswald, C. M. Trubey, et al. 2009. Effector memory T cell responses are associated with protection of rhesus monkeys from mucosal simian immunodeficiency virus challenge. *Nat. Med.* 15: 293–299.
37. Chen, W., L. C. Anton, J. R. Bennink, and J. W. Yewdell. 2000. Dissecting the multifactorial causes of immunodominance in class I-restricted T cell responses to viruses. *Immunity* 12: 83–93.
38. Spencer, J. V., and T. J. Braciale. 2000. Incomplete CD8$^+$ T lymphocyte differentiation as a mechanism for subdominant cytotoxic T lymphocyte responses to a viral antigen. *J. Exp. Med.* 191: 1687–1698.
39. Kaech, S. M., S. Hemby, E. Kersh, and R. Ahmed. 2002. Molecular and functional profiling of memory CD8 T cell differentiation. *Cell* 111: 837–851.
40. Sarkar, S., V. Kalia, W. N. Haining, B. T. Konieczny, S. Subramaniam, and R. Ahmed. 2008. Functional and genomic profiling of effector CD8 T cell subsets with distinct memory fates. *J. Exp. Med.* 205: 625–640.
41. Wherry, E. J., V. Teichgraber, T. C. Becker, D. Masopust, S. M. Kaech, R. Antia, U. H. von Andrian, and R. Ahmed. 2003. Lineage relationship and protective immunity of memory CD8 T cell subsets. *Nat. Immunol.* 4: 225–234.
42. Hulsmeyer, M., M. T. Fiorillo, F. Bettosini, R. Sorrentino, W. Saenger, A. Ziegler, and B. Uchanska-Ziegler. 2004. Dual, HLA-B27 subtype-dependent conformation of a self-peptide. *J. Exp. Med.* 199: 271–281.
43. Ruckert, C., M. T. Fiorillo, B. Loll, R. Moretti, J. Biesiadka, W. Saenger, A. Ziegler, R. Sorrentino, and B. Uchanska-Ziegler. 2006. Conformational dimorphism of self-peptides and molecular mimicry in a disease-associated HLA-B27 subtype. *J. Biol. Chem.* 281: 2306–2316.
44. Lovitch, S. B., T. J. Esparza, G. Schweitzer, J. Herzog, and E. R. Unanue. 2007. Activation of type B T cells after protein immunization reveals novel pathways of in vivo presentation of peptides. *J. Immunol.* 178: 122–133.
45. Yewdell, J. W., J. R. Bennink, and Y. Hosaka. 1988. Cells process exogenous proteins for recognition by cytotoxic T lymphocytes. *Science* 239: 637–640.
46. Cresswell, P., A. L. Ackerman, A. Giodini, D. R. Peaper, and P. A. Wearsch. 2005. Mechanisms of MHC class I-restricted antigen processing and cross-presentation. *Immunol. Rev.* 207: 145–157.
47. Dobano, C., W. O. Rogers, K. Gowda, and D. L. Doolan. 2007. Targeting antigen to MHC class I and class II antigen presentation pathways for malaria DNA vaccines. *Immunol. Lett.* 111: 92–102.
48. Kawashima, T., Y. Norose, Y. Watanabe, Y. Enomoto, H. Narazaki, E. Watari, S. Tanaka, H. Takahashi, I. Yano, M. B. Brenner, and M. Sugita. 2003. Cutting edge: major CD8 T cell response to live bacillus Calmette-Guerin is mediated by CD1 molecules. *J. Immunol.* 170: 5345–5348.
49. Germain, R. N., and D. H. Margulies. 1993. The biochemistry and cell biology of antigen processing and presentation. *Annu. Rev. Immunol.* 11: 403–450.
50. Sekaly, R. P. 2008. The failed HIV Merck vaccine study: a step back or a launching point for future vaccine development? *J. Exp. Med.* 205: 7–12.
51. Appay, V., D. C. Douek, and D. A. Price. 2008. CD8$^+$ T cell efficacy in vaccination and disease. *Nat. Med.* 14: 623–628.

Journal of Virological Methods 156 (2009) 162–165

Contents lists available at ScienceDirect

Journal of Virological Methods

journal homepage: www.elsevier.com/locate/jviromet

Short communication

Immunofluorescence imaging of the influenza virus M1 protein is dependent on the fixation method

Toshikatsu Shibata [a], Torahiko Tanaka [b], Kazufumi Shimizu [a,c], Satoshi Hayakawa [a,b], Kazumichi Kuroda [a,b,*]

[a] Division of Microbiology, Department of Pathology and Microbiology, Nihon University School of Medicine, 30-1 Oyaguchi-kami-cho, Itabashi-ku, Tokyo, 173-8610, Japan
[b] Division of Infectious Disease Control, Department of Advanced Medical Science, Nihon University School of Medicine, 30-1 Oyaguchi-kami-cho, Itabashi-ku, Tokyo, 173-8610, Japan
[c] Nihon University Advanced Research Institute for Sciences and Humanities, Open Research Center for Genome and Infectious Disease Control, Nihon University School of Medicine, 30-1 Oyaguchi-kami-cho Itabashi-ku, Tokyo, 173-8610, Japan

Article history:
Received 18 July 2008
Received in revised form 21 October 2008
Accepted 23 October 2008
Available online 9 December 2008

Keywords:
Influenza virus
M1 protein
Fixation method
Nuclear domain 10

A B S T R A C T

The distribution of the matrix (M1) protein of influenza virus in infected cells was examined using immunostaining. The fixation method influenced strongly the immunofluorescence pattern of the M1 protein. The M1 protein was distributed uniformly in both the cytoplasm and in nuclei when cells that had been infected with virus were fixed with paraformaldehyde. In cells that had been fixed with methanol, however, nuclear dots of the M1 protein were clearly visible. The dots were evident at 8 h post-inoculation. Up to 6 h post-inoculation, only a diffuse distribution of the M1 protein was observed. The dots were co-localized with promyelocytic leukemia (PML) protein, a major component of nuclear domain 10 (ND10), also called PML oncogenic domains (PODs) or PML-nuclear bodies (NBs). These results indicate that the nuclear dots of the M1 protein in cells that had been fixed with methanol are not artifacts of the fixation method. Furthermore, methanol fixation is preferred for localization of the influenza M1 protein in nuclei using immunostaining.

Influenza A virus matrix protein M1 is the most abundant protein in virions. It plays many important roles throughout the virus life cycle. By bridging the viral envelope and the ribonucleoprotein (RNP) complex, M1 is believed to maintain virion integrity (Noton et al., 2007; Schulze, 1972). The bridging interaction of the M1 protein is also assumed to be crucial in viral budding. The assumption is supported by a report that the M1 protein contains L (late) domain, which is expected to be involved in recruiting host components that are necessary for budding (Hui et al., 2006). Chen et al. (2007), however, reported that virus-like particles of influenza virus were formed without the M1 protein, which casts doubt on the necessity of the M1 protein for the budding process. Another important role of the M1 protein occurs at the stage of RNP export from the nucleus (Martin and Helenius, 1991). Binding of the M1 protein to the newly formed RNP complexes in the nucleus induces the export of RNP to the cytoplasm with the aid of NS2 (nuclear export protein, NEP), which is associated with the M1 protein (Akarsu et al., 2003; O'Neill et al., 1998; Yasuda et al., 1993). The regulation of viral RNA transcription by the M1 protein has also been described (Hankins et al., 1990; Watanabe et al., 1996).

A previous report (Sato et al., 2003) described co-localization of GFP-tagged influenza virus M1 protein (GFP-M1) with the promyelocytic leukemia (PML) protein, which is a major component of a subnuclear structure ND10 (nuclear domain 10), also called PML oncogenic domains (PODs) or PML-NBs (Hodges et al., 1998; Lamond and Earnshaw, 1998). The result suggests that the role of the M1 protein is related to the function of ND10. Several viral proteins localize to ND10; in fact, viral infection often changes it morphologically. Therefore, it is accepted widely that ND10 is involved in viral infection (Everett and Maul, 1994; Everett and Zafiropoulos, 2004; Hoppe et al., 2006).

Authentic M1 protein may also localize to ND10 in MDCK cells infected with influenza virus, as reported previously (Sato et al., 2003). That study described that nuclear dots were observed only after extraction of the infected cells using detergent and high salt, and for that reason, they might be interpreted as artifacts. The respective distributions of the M1 protein and the GFP-M1 protein in cells infected with virus were re-examined to investigate that interpretation.

* Corresponding author at: Division of Microbiology, Department of Pathology and Microbiology, Nihon University School of Medicine, 30-1 Oyaguchi-kami-cho, Itabashi-ku, Tokyo, 173-8610, Japan. Tel.: +81 3 3972 8111; fax: +81 3 3972 9560.
E-mail address: kkuroda@med.nihon-u.ac.jp (K. Kuroda).

0166-0934/$ – see front matter © 2008 Elsevier B.V. All rights reserved.
doi:10.1016/j.jviromet.2008.10.020

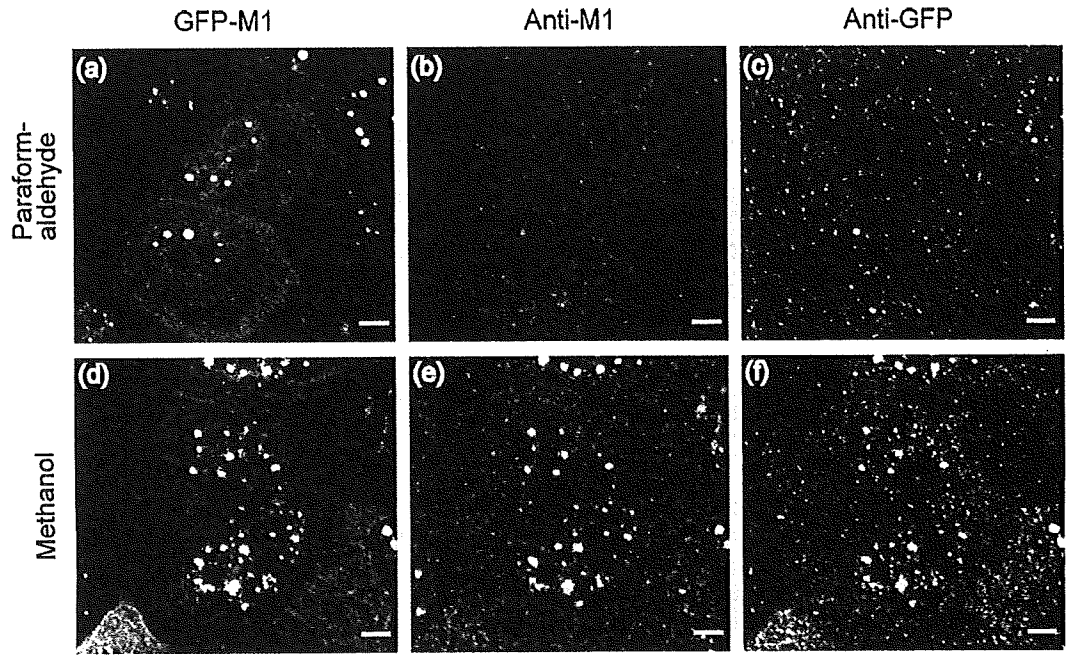

Fig. 1. Altered immunofluorescence patterns in differently fixed cells. MDCK-GFP/M1 5–6 cells were inoculated with influenza virus A/PR/8/34 at an MOI of 5. At 8 h post-inoculation, the cells were fixed with 4% paraformaldehyde (a–c) or methanol (d–f). The fixed cells were stained with anti-M1 rabbit serum (b and e) and anti-GFP antibody (c and f). They were then stained respectively with TRITC-conjugated anti-mouse IgG antibody and Alexa 647 conjugated anti-rabbit IgG antibody. Fluorescence of GFP-M1 was also observed (a and d). Bar, 5 μm.

To compare the distribution of the GFP-M1 protein with that of the M1 protein, MDCK-GFP/M1 5–6 cells that expressed stably the GFP-M1 protein were infected with influenza virus A/PR/8/34 for 8 h. The cells were fixed with 4% paraformaldehyde for 10 min at room temperature, permeabilized with 0.5% TritonX100, and stained with anti-M1 rabbit serum (kindly provided by M. Enami, Kanazawa University, Kanazawa, Japan) and with anti-GFP monoclonal antibody (JL-8; Clontech, CA, USA). The cells were then stained with Alexa 647-conjugated anti-rabbit IgG (Molecular Probes Inc., CA, USA) and tetramethyl rhodamine isothiocyanate (TRITC)-conjugated anti-mouse IgG antibody (Beckman Coulter Inc., CA, USA). Fluorescence was observed using a confocal microscope (FV1000; Olympus Corp., Tokyo, Japan). Nuclear dots of the GFP-M1 protein were observed clearly as reported previously, when the fluorescence of GFP was monitored (Fig. 1a) (Sato et al., 2003). In contrast, immunostaining with anti-M1 serum showed uniform fluorescence throughout the cytoplasm and the nucleus, except in the nucleolus (Fig. 1b). Although the absence of nuclear dots in staining with anti-M1 serum was explained in a previous report using coverage of the GFP-M1 protein with abundant authentic M1 proteins, another possibility was considered. The first and/or second antibody has insufficient access to the nuclear substructure, as suggested by a report describing inefficient immunostaining of ND10 in cells that had been fixed with paraformaldehyde (Negorev and Maul, 2001). The staining pattern with anti-GFP antibody would be expected to differ from the fluorescence pattern of GFP-M1 in MDCK-GFP/M1 5–6 cells infected with influenza virus if that were the case. As shown in Fig. 1c, anti-GFP antibody staining did not show nuclear dots, in contrast to the fluorescence pattern of GFP-M1 (Fig. 1a and c). The result was not explained using the alteration of the epitope structure recognized by the anti-GFP antibody JL-8 because diffuse staining of the anti-GFP antibody was observed clearly in the cytoplasm of infected cells (Fig. 1c). No clear difference of patterns was found between anti-GFP antibody staining and fluorescence of the GFP-M1 protein in mock-inoculated cells (data not shown). Instead, the result will show that antibodies do not access ND10 easily in cells that had been fixed with paraformaldehyde.

The immunostaining pattern is altered depending on multiple factors. An important factor is the fixation method: many epitopes are masked or altered using certain fixatives (Harlow and Lane, 1988). To examine the influence of fixation, fixation was attempted using an organic solvent, methanol, instead of a cross-linking reagent, paraformaldehyde. The A/PR/8/34 infected MDCK-GFP/M1 5–6 cells were fixed with methanol for 5 min at −20 °C and were stained with the anti-GFP antibody JL8 and anti-M1 serum. In contrast to the staining of cells that had been fixed with paraformaldehyde, staining of methanol-fixed cells with JL8 showed clear nuclear dots; the dots were superimposable on those of GFP-fluorescence of GFP-M1 (Fig. 1d and f). Anti-M1 staining also revealed clear nuclear dots (Fig. 1e). These results demonstrated that methanol fixation yields ND10 that is more accessible by antibodies than that created by paraformaldehyde fixation. The results also confirmed that nuclear dots of the M1 protein were not observed in cells that had been fixed with paraformaldehyde, with subsequent permeabilization using methanol (data not shown). In previous reports on the interaction between ND10 and viral proteins, both paraformaldehyde fixation and organic solvent fixation were used (Borden et al., 1998; Choi et al., 2003; Doucas et al., 1996; Herzer et al., 2005; Murges et al., 2001; Young et al., 2002).

Based on the results described above, the distribution pattern of authentic M1 protein in cells that had been infected with influenza virus and fixed with methanol was examined again. The MDCK cells were infected with A/PR/8/34 and were fixed with methanol. They were then stained with anti-M1 serum at various times after inoculation. Although nuclear dots were not observed until 6 h post-inoculation, clear dots of the M1 protein were detected in nuclei of methanol-fixed cells at 8 h and thereafter post-inoculation (Fig. 2). The nuclear dot staining of the M1 protein in methanol-fixed cells might not be an artifact produced by methanol fixation:

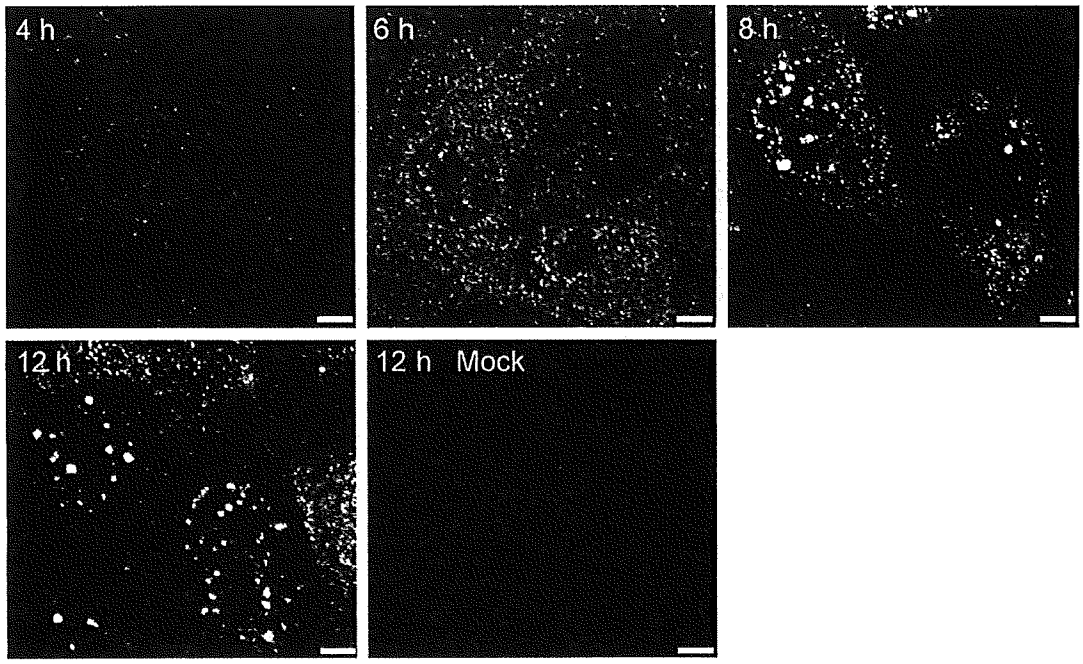

Fig. 2. Time course of the immunofluorescence pattern of the M1 protein in influenza virus infected cells. The MDCK cells were inoculated using A/PR/8/34 at an MOI of 5 or were mock-inoculated. At the indicated times post-inoculation, the cells were fixed with methanol. The fixed cells were stained with anti-M1 rabbit serum. Then they were stained with Alexa 488 conjugated anti-rabbit IgG antibody. Mock-treated cells were fixed at 12 h post-inoculation. Bar, 5 μm.

uniform staining was observed until 6 h post-inoculation. Some authentic M1 protein accumulated in the nuclear subcompartment, very likely into ND10, as suggested in a previous report (Sato et al., 2003).

To confirm the accumulation of the M1 protein into ND10, human PML isoform 4 was cloned into the BamHI site of pJRed-N vector (Evrogen, Moscow, Russia) to construct the expression vector of JRed-PML fusion protein (pJRed-PML). The MDCK cells were transfected with pJRed-PML and were infected with A/PR/8/34. At 12 h post-inoculation, these cells were fixed with methanol and stained with anti-M1 rabbit serum, with subsequent staining with Alexa488-conjugated anti-rabbit IgG antibody. In the stained cells, nuclear dots of JRed-PML fluorescence corresponding to ND10 were observed clearly. Staining with anti-M1 also showed nuclear dots. The dots of the M1 protein were co-localized with those of JRed-PML (Fig. 3). The results confirmed accumulation of authentic M1 protein into ND10 during influenza virus infection.

Localization of the M1 protein to ND10 is assumed to be necessary for the progress of the infection to the late phase. Although the role of ND10 remains controversial, several reports describe that ND10 contributes to the antiviral response of host cells (Everett and Chelbi-Alix, 2007; Everett et al., 2006; Pampin et al., 2006). Influenza virus is an example of many viruses whose infection is influenced by PML, a major component of ND10. Overexpression of PML isoform 3 inhibits replication of influenza virus (Chelbi-Alix et al., 1998), and depletion of PML by siRNA engenders enhanced viral propagation (Iki et al., 2005). The accumulation of the M1 protein to ND10 might prevent the anti-influenza virus effect of PML and accelerate progression of the infection process. Another possibility is that the accumulation of the M1 protein might result from the anti-viral activity of ND10; M1 is inactivated in ND10 and the concentration of functional M1 protein in nucleoplasm is reduced.

It must be emphasized that methanol fixation should be chosen to localize the M1 protein in nuclei using immunostaining and

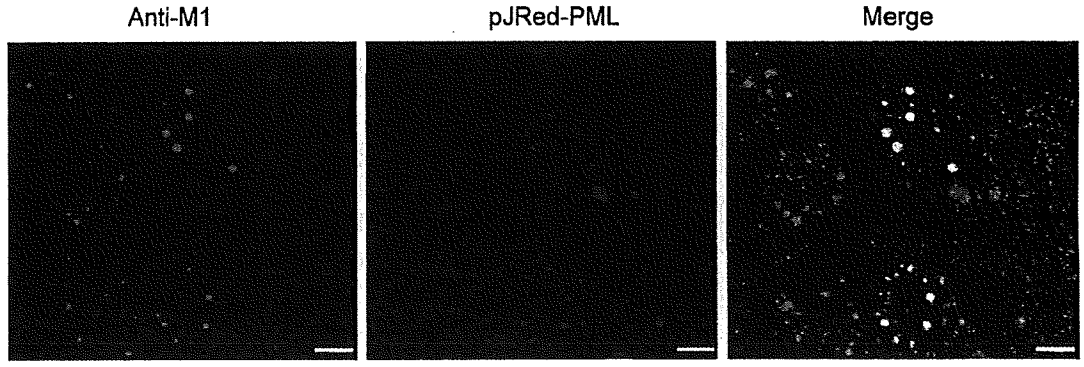

Fig. 3. Co-localization of the M1 protein with PML. MDCK cells were transfected with pJRed-PML. At 24 h post-transfection, they were inoculated with A/PR/8/34 at MOI 5. The inoculated cells were fixed with methanol at 8 h post-inoculation and were stained with anti-M1 rabbit serum. They were then stained with Alexa 488 conjugated anti-rabbit IgG antibody. Fluorescence of JRed-PML was also observed. A merged image of immunostaining and JRed-PML is shown (Merge). Bar, 5 μm.

that the same will be true for nuclear proteins of other viruses. Finally, the influence of fixation methods on nuclear proteins other than the M1 protein should be noted. Immunostaining of another influenza viral protein, NS1, a nucleolar protein, nucleolin, and two ND10-resident proteins, PML and Daxx, was attempted. The staining pattern of the NS1 protein and nucleolin was affected by the fixation method (Murayama et al., 2007). The pattern of the PML protein and the Daxx protein was not affected. Because it is difficult to predict the effect of fixation, it is recommended to attempt both paraformaldehyde fixation and methanol fixation methods for examination of the distribution of nuclear proteins using immunostaining.

Acknowledgements

This work was supported by a grant from the Ministry of Education, Culture, Sports, Science and Technology to promote open research for young academics and specialists. Masayoshi Enami (Kanazawa University) is appreciated for kind provision of anti-M1 rabbit serum.

References

Akarsu, H., Burmeister, W., Petosa, C., Petit, I., Müller, C., Ruigrok, R., Baudin, F., 2003. Crystal structure of the M1 protein-binding domain of the influenza A virus nuclear export protein (NEP/NS2). EMBO J. 22, 4646–4655.

Borden, K.L.B., Dwyer, E.J.C., Salvato, M.S., 1998. An arenavirus RING (zinc-binding) protein binds the oncoprotein promyelocyte leukemia protein (PML) and relocates PML nuclear bodies to the cytoplasm. J. Virol. 72, 758–766.

Chelbi-Alix, M.K., Quignon, F., Pelicano, L., Koken, M.H., de The, H., 1998. Resistance to virus infection conferred by the interferon-induced promyelocytic leukemia protein. J. Virol. 72, 1043–1051.

Chen, B.J., Leser, G.P., Morita, E., Lamb, R.A., 2007. Influenza virus hemagglutinin and neuraminidase, but not the matrix protein, are required for assembly and budding of plasmid-derived virus-like particles. J. Virol. 81, 7111–7123.

Choi, J., Chang, J.S., Song, M.S., Ahn, B.Y., Park, Y.I., Lim, D.S., Han, Y.S., 2003. Association of hepatitis B virus polymerase with promyelocytic leukemia nuclear bodies mediated by the S100 family protein p11. Biochem. Biophys. Res. Commun. 305, 1049–1056.

Doucas, V., Ishov, A.M., Romo, A., Juguilon, H., Weitzman, M.D., Evans, R.M., Maul, G.G., 1996. Adenovirus replication is coupled with the dynamic properties of the PML nuclear structure. Genes Dev. 10, 196–207.

Everett, R., Chelbi-Alix, M., 2007. PML and PML nuclear bodies: implications in antiviral defence. Biochimie 89, 819–830.

Everett, R., Maul, G., 1994. HSV- 1 IE protein Vmw110 causes redistribution of PML. EMBO J. 13, 5062–5069.

Everett, R., Rechter, S., Papior, P., Tavalai, N., Stamminger, T., Orr, A., 2006. PML contributes to a cellular mechanism of repression of herpes simplex virus type 1 infection that is inactivated by ICP0. J. Virol. 80, 7995–8005.

Everett, R., Zafiropoulos, A., 2004. Visualization by live-cell microscopy of disruption of ND10 during herpes simplex virus type 1 infection. J. Virol. 78, 11411–11415.

Hankins, R., Nagata, K., Kato, A., Ishihama, A., 1990. Mechanism of influenza virus transcription inhibition by matrix (M1) protein. Res. Virol. 141, 305–314.

Harlow, E., Lane, D., 1988. Cell staining. In: Antibodies. Cold Spring Harbor Laboratory Press, Cold Spring Harbor, New York, pp. 359–420.

Herzer, K., Weyer, S., Krammer, P.H., Galle, P.R., Hofmann, T.G., 2005. Hepatitis C virus core protein inhibits tumor suppressor protein promyelocytic leukemia function in human hepatoma cells. Cancer Res. 65, 10830–10837.

Hodges, M., Tissot, C., Howe, K., Grimwade, D., Freemont, P., 1998. Structure, organization, and dynamics of promyelocytic leukemia protein nuclear bodies. Am. J. Hum. Genet. 63, 297–304.

Hoppe, A., Beech, S., Dimmock, J., Leppard, K., 2006. Interaction of the adenovirus type 5 E4 Orf3 protein with promyelocytic leukemia protein isoform II is required for ND10 disruption. J. Virol. 80, 3042–3049.

Hui, E., Barman, S., Tang, D., France, B., Nayak, D., 2006. YRKL sequence of influenza virus M1 functions as the L domain motif and interacts with VPS28 and Cdc42. J. Virol. 80, 2291–2308.

Iki, S., Yokota, S., Okabayashi, T., Yokosawa, N., Nagata, K., Fujii, N., 2005. Serum-dependent expression of promyelocytic leukemia protein suppresses propagation of influenza virus. Virology 343, 106–115.

Lamond, A., Earnshaw, W., 1998. Structure and function in the nucleus. Science 280, 547–553.

Martin, K., Helenius, A., 1991. Nuclear transport of influenza virus ribonucleoproteins: the viral matrix protein (M1) promotes export and inhibits import. Cell 67, 117–130.

Murayama, R., Harada, Y., Shibata, T., Kuroda, K., Hayakawa, S., Shimizu, K., Tanaka, T., 2007. Influenza A virus non-structural protein 1 (NS1) interacts with cellular multifunctional protein nucleolin during infection. Biochem. Biophys. Res. Commun. 362, 880–885.

Murges, D., Quadt, I., Schroer, J., Knebel-Morsdorf, D., 2001. Dynamic nuclear localization of the baculovirus proteins IE2 and PE38 during the infection cycle: the promyelocytic leukemia protein colocalizes with IE2. Exp. Cell. Res. 264, 219–232.

Negorev, D., Maul, G., 2001. Cellular proteins localized at and interacting within ND10/PML nuclear bodies/PODs suggest functions of a nuclear depot. Oncogene 20, 7234–7242.

Noton, S., Medcalf, E., Fisher, D., Mullin, A., Elton, D., Digard, P., 2007. Identification of the domains of the influenza A virus M1 matrix protein required for NP binding, oligomerization and incorporation into virions. J. Gen. Virol. 88, 2280–2290.

O'Neill, R., Talon, J., Palese, P., 1998. The influenza virus NEP (NS2 protein) mediates the nuclear export of viral ribonucleoproteins. EMBO J. 17, 288–296.

Pampin, M., Simonin, Y., Blondel, B., Percherancier, Y., Chelbi-Alix, M., 2006. Cross talk between PML and p53 during poliovirus infection: implications for antiviral defense. J. Virol. 80, 8582–8592.

Sato, Y., Yoshioka, K., Suzuki, C., Awashima, S., Hosaka, Y., Yewdell, J., Kuroda, K., 2003. Localization of influenza virus proteins to nuclear dot 10 structures in influenza virus-infected cells. Virology 310, 29–40.

Schulze, I., 1972. The structure of influenza virus. II. A model based on the morphology and composition of subviral particles. Virology 47, 181–196.

Watanabe, K., Handa, H., Mizumoto, K., Nagata, K., 1996. Mechanism for inhibition of influenza virus RNA polymerase activity by matrix protein. J. Virol. 70, 241–247.

Yasuda, J., Nakada, S., Kato, A., Toyoda, T., Ishihama, A., 1993. Molecular assembly of influenza virus: association of the NS2 protein with virion matrix. Virology 196, 249–255.

Young, P.J., Jensen, K.T., Burger, L.R., Pintel, D.J., Lorson, C.L., 2002. Minute virus of mice NS1 interacts with the SMN protein, and they colocalize in novel nuclear bodies induced by parvovirus infection. J. Virol. 76, 3892–3904.